TRENDS IN SCIENCES 2025; 22(9): 10416
https://doi.org/10.48048/tis.2025.10416
RESEARCH ARTICLE

Synthesis, Characterization, Cyclic Voltammetry (CV), Theoretical Molecular Docking against Breast Cancer and Computational Study to Determine the Energy Gap of a Newly Series of Organotillium Compounds Based on N-(4-Benzoylphenyl)–2–Tellerocyanatoacetamide

Ahmed Mohammed Alsanafi and Nuha Hussain Al-Saadawy*

Department of Chemistry, College of Science, University of Thi-Qar, Nasiriyah, Thi-Qar 64001, Iraq

(*Corresponding author's e-mail: Nuh.hussain@sci.utq.edu.iq)

Received: 20 April 2025, Revised: 21 May 2025, Accepted: 1 June 2025, Published: 10 July 2025

Abstract

The purposes of the present study, scale up a new series of tellurium compounds based on N-(4-benzoylphenyl)-2-chloroacetamide (4-CAP), Tellurium metal (Te), potassium cyanide (KCN) & dimethyl sulfoxide (DMSO) as a solvent. This reaction is carried out in an inert atmosphere in the argon gas (Ar) is needed to get N-(4-benzoylphenyl)-2-Tellerocyanatoacetamide; beyond this, derivatives are synthesized, and organyl tellurium trihaleds. All synthesized compounds were characterized by (FT-IR), (1H-NMR) & mass spectroscopies. The spectroscopic data were in good agreement with the proposed chemical structures of the synthesized compounds. The cyclic voltammetry of all synthesized and characterized compounds was scanned at 0.1 and 0.3 v/s. To track the number of redox states in each compound, determine the required potential for each reaction, find the potential difference and get the anodic/cathodic current ratio. To generate 3D structures of the newly compounds for molecular docking, Chemdraw software files were converted and used after energy minimization. The files were preoptimized with semiempirical AM1 method using Hyperchem 8.08 software files. The files were optimized using density functional theory (DFT) method with the B3LYP/6-31G basis set which is well proven for describing the most stable conformation and used to calculate global reactivity descriptors through Gaussian 09 also. All of these have some default values before achieving "YES". Density functional theory (DFT) calculations were used to study the molecular structures of the synthesized organotellurium compounds. The geometry, HOMO, LUMO, and energy gap were generated from calculations of optimized structures. Comparing the HOMO energies, it was possible to study the donor and acceptor properties of the prepared organotillurium compounds. Finally, several important chemical properties such as electronegativity, electrophilicity, ionization potential, and electron affinity were calculated and discussed.

Keywords: Organotllurium, Cyclic voltammetry cyclic voltammetry, Molecular docking, Burst cancer, DFT, HOMO, LUMO

Introduction

Tellurium (Te) possesses remarkable properties that enable its use in a diverse range of applications. It exhibits excellent electrical, optical, and thermal conductivities, along with asymmetry that affects its electrical responses. As a p-type semiconductor with a finite band gap, bulk Te is particularly useful in gas sensors, solar cells, and transistors, thanks to its additional characteristics such as optical conductivity and thermoelectric properties. Furthermore, its strong sensitivity to infrared radiation positions monolayer 2D Te as a promising candidate for various optoelectronic applications [1-4]. Telluriocyanate, a compound containing tellurium and an isocyanate group, has been extensively researched and synthesized in various forms alongside other tellurium compounds. These compounds have unique properties that make them

suitable for a wide range of applications. Research has primarily focused on the synthesis of organotellurium compounds, particularly those containing pyrazole derivatives, such as 3,5-dimethyl-1-phenyl-4-tellurocyanate and pentadiene-2,4-dione-3-tellurocyanate. Furthermore, research into tellurium pseudohalides has resulted in the development of compounds such as tellurium tetrazide and tellurium cyanides, thereby improving our understanding of tellurium chemistry. The importance of organotellurium compounds is largely due to their ability to treat infections, which is influenced by their organic structure, covalent nature, and unique properties [5-8]. Tellurium trihalides are compounds formed by the combination of tellurium and three halogen atoms, exhibiting various structural and chemical characteristics depending on the halogens involved. Early studies indicated that aryl tellurium trihalides might act as weak electrolytes in solvents such as DMSO and DMF, with their conductivities analyzed using Foss-Hsieh and Bethe equations. Further research has uncovered a range of tellurium compounds, including pseudo-tellurium halides, which possess unique properties and structures. Notably, researchers from the Department of Chemistry at the University of Thi-Qar have successfully synthesized a variety of telluriocyanate compounds and tellurium trihalides, including [9-nitro-10-tellurocyanato-9-10-dihydroanthracene] and its derivatives with chlorine, bromine, and iodine [9-13]. Density Functional Theory (DFT) is a powerful computational tool widely used in physics and chemistry for determining the electronic structure of atoms and molecules. Its high predictive accuracy allows for calculations that closely align with experimental observations, making it invaluable for research. Advances in computational capabilities have expanded DFT's applicability, enabling collaborative efforts between experimental and computational investigations, particularly in complex systems. Overall, DFT serves as a fundamental theoretical framework in modern computational chemistry, physics, and materials science, playing a crucial role in bridging theory and practical applications [14-17]. Cyclic voltammetry (CV) is a valuable technique for analyzing the current-potential properties of various reactions and materials, particularly in the study of the hydrogen evolution reaction. This method allows for the measurement of exchange current through hydrogen adsorption free energy derived from density functional theory. Additionally, CV is instrumental in investigating the electrochemical deposition of selenium on carbon-supported Pt nanoparticles, providing insights into surface site availability and the structure-function relationship of nanostructured materials. The application of CV extends to the characterization of supercapacitors and the analysis of organic compounds [18], which is crucial for the development of stable organic electronic devices in a rapidly growing field [19-24]. Molecular docking is a key computational method in drug discovery, primarily used to predict interactions between small molecules, or ligands, and target proteins. This technique aids in identifying optimal ligand orientations that lower the free energy of stable complexes, making it crucial for developing targeted cancer therapies. Recent advancements in artificial intelligence, including advanced algorithms, neural networks, and reinforcement learning, have significantly enhanced the efficiency and accuracy of molecular docking predictions. Additionally, molecular docking plays a vital role in virtual screening, allowing scientists to analyze extensive compound libraries and design lead compounds effectively, thereby accelerating the drug discovery process and addressing various health conditions, including cancer [25-30].

Materials and methods

A series of tellurium compounds were prepared based on the N-(4-benzoylphenyl)-2-chloroacetamide (4-CAP), as shown below [31]. As shown in **Scheme 1**, physical properties shown in **Table 1**.

Preparation of N-(4-benzoylphenyl)-2-chloroacetamide (CAP)

In a round bottom flask, a solution of (10 mmol, 1.97 g) 4-aminobenzophenone (A.B.P) was dissolved in 10 mL of glacial acetic acid (G.A.A) with continuous stirring at room temperature. A solution of (14 mmol, 0.8 mL) Chloroacetylchloride (C.A.C) was gradually added by an addition funnel with continuous stirring for 30 min at room temperature. Then, 10 mL of 0.5 M sodium acetate (5 mmol, 0.41 g) was added dropwise, a precipitate was observed with each drop with continuous stirring for another 30 min at room temperature. Then, white crystals of N-(4-benzoylphenyl)-2-

chloroacetamide (C.A.P) was filtered, washed several times with deionized water, dried and recrystallized using absolute ethanol, the purity was monitored by TLC, Rf value = 0.68 (3-n-hexane: 7-ethyl acetate), melting point 123 - 125 °C, yield 87%. FT-IR using KBr: υ (NH) = 3,350 cm^{-1} [32], υ (C–H) Aromatic = 3,087 cm^{-1}, υ (C–H) Aliphatic = 2,954 cm^{-1} ,υ (C=O) Ketone = 1,703 cm^{-1} [33], υ (C=O) Amide = 1,638 cm^{-1}, υ (C=C) Aromatic = 1,596 cm^{-1}, (C–N) = 1,316 cm^{-1}, (C–Cl) = 728 cm^{-1}. ^{1}H- NMR (400 MHz, DMSO- d6) δ H_20, H_{21}(4.33ppm, s,2H), Ar-H (7.53 - 781 ppm, m, 9H), H_{16} (10.71 ppm, s,1H). ^{13}C-NMR (400 MHz, DMSO-d6) at ppm C_1 = 44.10, C_2 = X, C_6 = 137.89, C_7 = 132.77, C_9 = 143.04, C_3 = 16571, C_4 = 195.01, C_5 = 131.67, C11 = 129.88, C_8 = 119.11, C_{10} = 128.95 as shown in **Tables 2 - 4** and **Figures 1 - 3** and **8**.

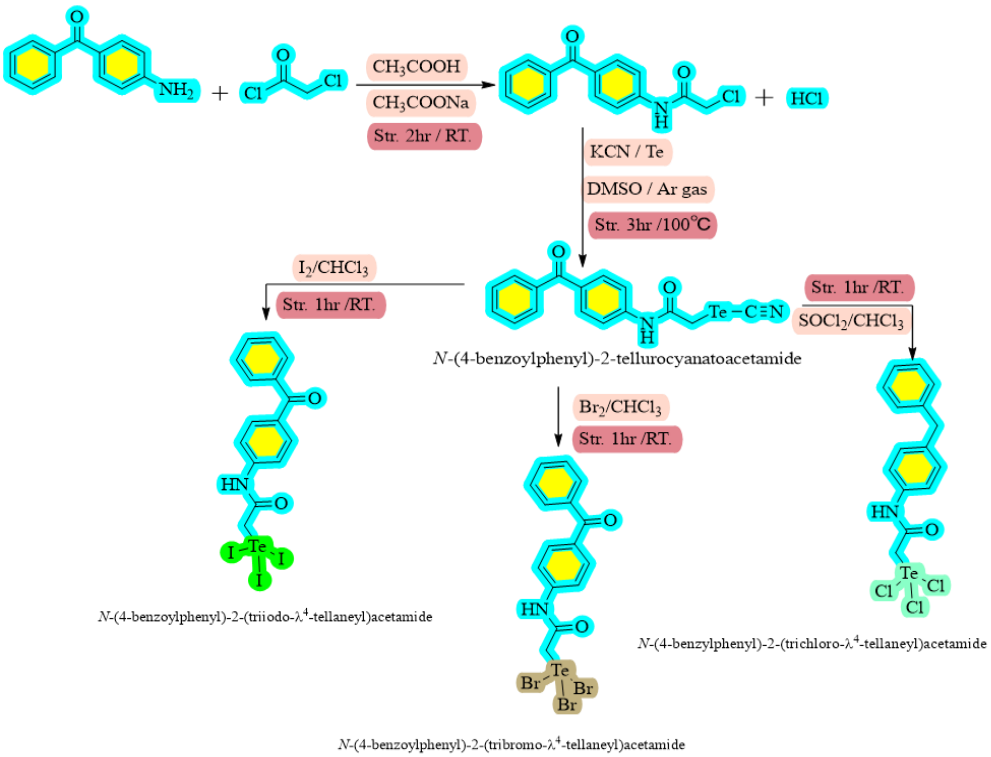

Scheme 1 Preparing N-(4-benzoylphenyl)-2-tellurocyanatoacetamide CAP-Te-CN and its trihalides derivatives.

Preparation of N-(4-benzoylphenyl)-2-tellurocyanatoacetamide CAP-Te-CN

This compound was prepared by the same way as for compound CAP- Se- CN and under the same condition by adding (5.6 mmol, 0.7 g) of tellurium Te, a precipitate with a pale-yellow color was obtained with a Rf values = 0.81 (3-hexane: 7-ethyl acetate), melting point (135 - 137 °C), and a yield (1.4 g, 63%). FT-IR using KBr: υ (NH) = 3,284 cm^{-1}[34], υ (C–H) Aromatic = 3,098 cm^{-1}, υ (C–H) Aliphatic = 2,959 cm^{-1}, (C ≡ N) = 2,142 cm^{-1} [35], υ (C=O) Ketone = 1,677 cm^{-1}, υ (C=O) Amide = 1,655 cm^{-1}, υ (C=C) Aromatic = 1,590 cm^{-1}, υ (C–N) = 1,316 cm^{-1} , υ (C–Te) = 475 cm^{-1} [36-39] ^{1}H NMR (400 MHz, DMSO-d6) δ H_{24} (3.72ppm ,s,1H), H_{23} (4.14 ppm, s, 1H), Ar-H (7.51 - 7.95 ppm, m, 9H), H_{16} (46 ppm, 11.39 ppm, d, 1H). ^{13}C NMR (400 MHz, DMSO-d6) ppm C_1 = 7.69, C_2 = 118.71, C_6, C_7 = 138.01, C_9 = 143.89, C_3 = 172.44, C_4 = 194.68, C_5 = 131.68, C_{11} = 132.70, C_8 = 128.94, C_{10} = 129.86 as shown in **Tables 2 - 4** and **Figures 1, 2, 4** and **9**.

Preparing tri halides

Preparing N-(4-benzoylphenyl)-2-(trichloro-l4-tellaneyl)acetamide CAP-Te- Cl_3

In a 100 mL beaker, dissolve (25 mmol, 1g) of N-(4-benzoylphenyl)-2-tellurocyanatoacetamide CAP-Te-CN in (25 mL) of chloroform and add (25 mmol 0.18 mL) of $SOCl_2$ solution in chloroform with continuous stirring for 2 h and pour into a Petri- dish and leave overnight to allow the solvent to evaporate, leaving a sticky precipitate was treated by re- dissolving with DMSO and filtering the solution, then pouring it into

ice- cold deionized water, white crystals was formed, washed several times with deionized water, filtered and drying. Purity was monitored by TLC, Rf = 87(3-hexan:7-ethylacetate), melting point (88 - 90 ℃), and a yield (37 %). FT-IR using KBr: υ (NH) = 3,294 cm^{-1} [40], υ (C– H) Aromatic = 3,056 cm^{-1}, υ (C– H) Aliphatic= 2,928 cm^{-1}, υ (C=O) Ketone and υ (C=O) Amide = 1,653 Broad cm^{-1}, υ (C=C) Aromatic = 1,597 cm^{-1}, υ (C–N) = 1,318 cm^{-1} , υ (C–Te) = 514 cm^{-1} [41]. ^{1}H NMR (400 MHz, DMSO-d6) δ H_{24}, H_{25} (3.60 ppm, s, 2H), Ar-H (7.52 - 7.78 ppm, m, 9H), H_{16} (10.57 ppm, s, 1H). ^{13}C NMR (400 MHz, DMSO- d6) ppm C_1 = 24.68, C_2 = X, C_6 = 137.89, C_7 = 132.72, C_9 = 142.83, C_3 = 165.76, C_4 = 195.07, C_5 = 131.66, C_{11} = 129.86, C_8 = 119.33, C_{10} = 128.93 as shown in **Tables 2 - 4** and **Figures 1, 2, 5** and **10**.

Preparing N-(4-benzoylphenyl)-2-(tribromo-l4-tellaneyl) acetamide CAP-Te- Br_3

This compound was prepared by the same way as for compound CAP- Te- Cl_3 and under the same condition by adding (25 mmol 0.13 mL) of Bromine solution in chloroform white crystals was formed, Rf = 95 (3-hexan:7-ethylacetate), melting point (76 - 78 ℃), and a yield (33 %). FT-IR using KBr: υ (NH) = 3,264 cm^{-1} [42], υ (C–H) Aromatic = 3,118 cm^{-1}, υ (C–H) Aliphatic = 2,982 cm^{-1}, υ (C=O) Ketone = 1,670 cm^{-1}, υ (C=O) Amide = 1,651 cm^{-1}, υ (C=C) Aromatic = 1,597 cm^{-1}, υ (C–N) = 1,311 cm^{-1} , υ (C–Te) = 504 cm^{-1} [41]. 1H NMR (400 MHz, DMSO-d6) δ H_{24}, H_{25}(4.06 ppm, 4.12 ppm, d, 2H), Ar-H (7.53 - 8.01 ppm, m, 9H), H_{16} (10.85 ppm, s, 1H). ^{13}C NMR (400 MHz, DMSO- d6) ppm C_1 = 30.79, C_2 = X, C_6 =137.87, C_7 = 132.82, C_9 = 143.16, C_3 = 165.92, C_4 = 195.03, C_5 = 131.70, C_{11} = 129.90, C_8 = 119.29, C_{10} = 128.98 as shown in **Tables 2 - 4** and **Figures 1, 2, 6** and **11**.

Preparing N-(4-benzoylphenyl)-2-(triiodo-l4-tellaneyl) acetamide CAP-Te- I_3

This compound was prepared by the same way as for compound CAP- Se- CN and under the same condition by adding (25 mmol 0.63 g) of Iodine solution in chloroform, dark brown crystals was formed, Rf = 83 (3-hexan:7-ethylacetate), melting point (139 - 141 ℃), and a yield (33%). FT-IR using KBr: υ (NH) = 3,285 cm^{-1} [40], υ (C–H) Aromatic = 3,053 cm^{-1}, υ (C–H) Aliphatic= 2,927 cm^{-1}, υ (C=O) Ketone = 1,654 cm^{-1}, υ (C=O) Amide = 1,637 cm^{-1}, υ (C=C) Aromatic = 1,593 cm^{-1}, υ (C–N) = 1,317 cm^{-1} , υ (C–Te) = 510 cm^{-1} [41]. 1H NMR (400 MHz, DMSO-d6) δ H_{24}, H_{25} (4.11 ppm, s, 2H), Ar-H (7.54 - 7.92 ppm, m, 9H), H_{16} (10.82 ppm, s, 1H). ^{13}C NMR (400 MHz, DMSO- d6) ppm C_1 = 30.79, C_2 = X, C_6 = 137.87, C_7 = 132.82, C_9 = 143.16, C_3 = 165.92, C_4 = 195.03, C_5 = 131.70, C_{11} = 129.90, C_8 = 119.29, C_{10} = 128.98 as shown in **Tables 2 - 4** and **Figures 1,2,7** and **12**.

Table 1 physical properties of prepared compounds.

NO	Compound	Molecular weight	color	Melting point ℃	Yield %
1	ABP	197.2370	White yellowish	122 - 124	-
2	CAP	273.7160	white	123 - 125	87%
3	CAP-Te-CN	391.8840	Yellowish brown	135 - 137	63%
4	CAP-Te-Cl_3	472.2160	white	88 - 90	37%
5	CAP-Te-Br_3	605.5780	dark brown	76 - 78	33%
6	CAP-Te-I_3	746.5794	Dark brown	139 - 141	33%

Study of electrochemistry

Looking at cyclic voltammetry (CV)

Cyclic voltammetry 1 1mM scans were used to carry out the electrochemical investigation of the synthesized compounds. The solvent of dimethylformamide was characterized using 0.1 M tetra-n-butylammonium perchlorate ($(CH3)4N^{+}ClO4^{-}$), TBAP, as the supporting electrolyte within the range 0.0 to −2.5 V at room temperature for all compounds. The scans were conducted in the positive direction from +2.0 to −2.5 V at a scan rate of 100 mV/s for the negative scan and 300 mV/s for the positive scan. In the studied

range, the cyclic voltammetry measurements of the compounds, which are non- electrochemically reversible, gave multiple redox peaks.

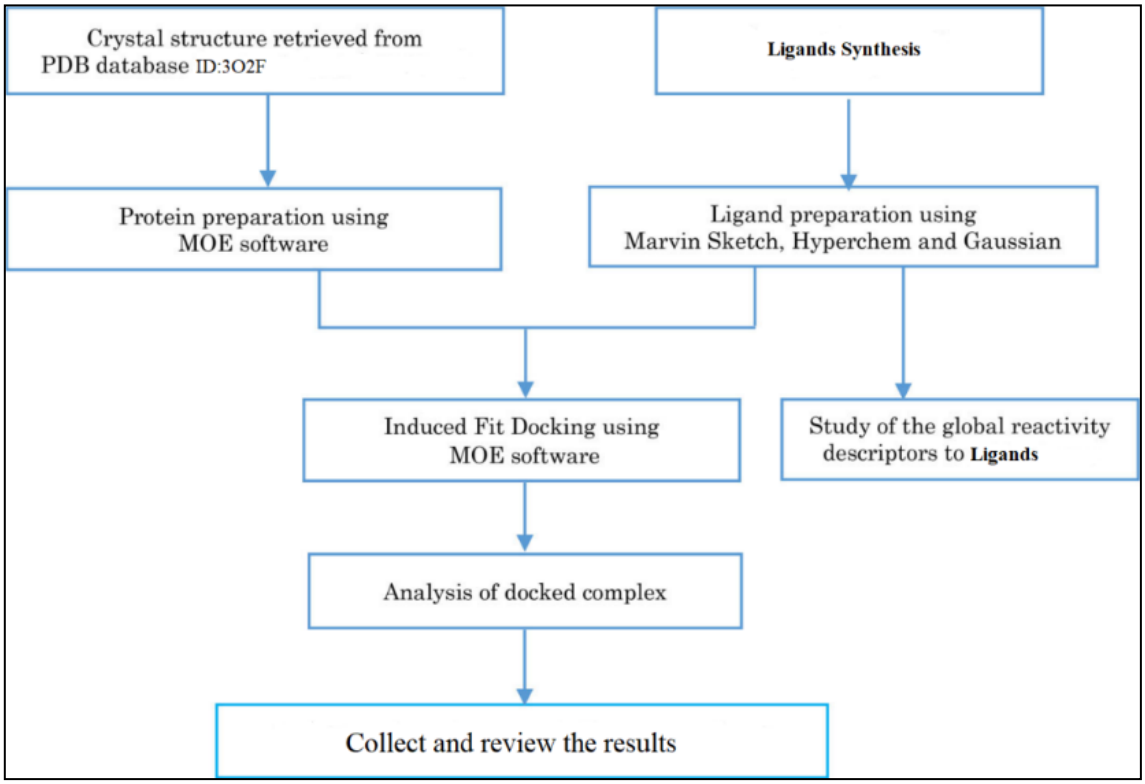

Scheme 2 Schematic representation of the docking procedure, analysis of drugs and reactivity.

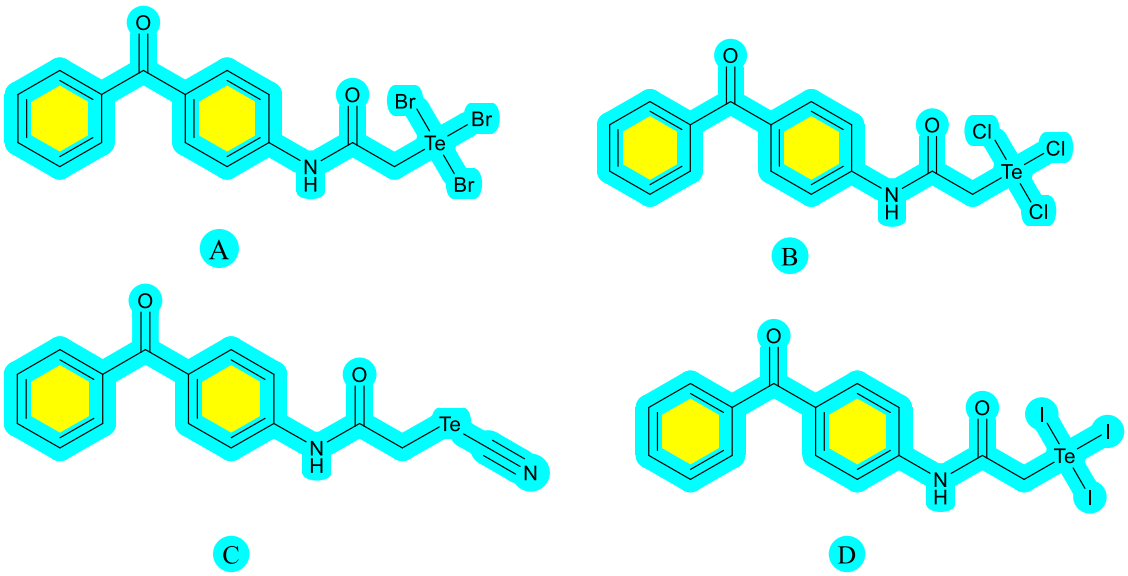

Figure 25 The structures of selected compounds.

Molecular docking

Preparing a molecules library

The newly synthesized compounds (A, B, C and D) were characterized and used in the molecular docking process. 3D structures of the compounds (A, B, C and D) were generated by Chemdraw Ultra 12. 0 software and then energy minimization was carried out. The structures were pre- optimized with the semi-

empirical AM1 method using Hyperchem 8.08 software [43]. Thereafter, the structures were optimized using the B3LYP/6-31G basis set under DFT method that was employed to find the most stable conformation, further used for the calculation of the global reactivity descriptors through Gaussian 09. All values are positive after calculation vibrational frequencies to drugs, those results indicate that the drugs are stable. The optimized structures were combined in one database on MOE software to study the affinity of ligands. Also, (**Scheme 2**) illustrates the schematic representation of the docking procedure, analysis of drugs, and reactivity.

Receptor preparation

The crystal structures Structure of the N-domain of GRP94 bound to the HSP90 inhibitor PU-H54 (PDB ID: 3O2F) **Figure 26**. were chosen from the Protein Data Bank. Since the water molecule in the active site of the target enzyme is critical, it was placed in the active sites to ensure making a hydrogen bond between the ligand and the target. Thereafter the protein structure was prepared by fixing the missing bonds that were broken in X-ray diffraction, and then the hydrogen atoms were added. Also very important, PDB is a legitimate source for the crystal structure of biological macromolecules, globally.

Component-target molecular docking

All docking and scoring calculations were performed using the molecular operation environment software (MOE) (Molecular Operating Environment (MOE), 2015). Crystal structure data for the N-domain of GRP94 bound to PU-H54, a specific inhibitor of HSP90, was obtained from the Protein Data Bank with an ID of 3O2F (**Figure 26)**, resolved at 2.50 Å. A resolution between 1.4 and 2.5 Å is rather good for quality in docking studies. It is a common fact that the best RMSD values must be nearly 2 Å with energy ≤ −7 kcal/mol. These two values are common to set for checking the result of molecular docking.

Computational study

The study evaluated the effectiveness of a method in characterizing the properties of compounds in the gas phase. Quantum calculations were conducted using Density Functional Theory (DFT) at the hybrid B3LYP level, which integrates various exchange correlation methods. The compounds' electronic properties and geometric structures were analyzed with a 3 - 21 G basis set and Gaussian software, while their reactivity and stability were assessed through DFT-based descriptors using specific mathematical equations [43-50].

Results and discussion

FT-IR spectra

The CAP spectrum was distinguished from the ABP spectrum by the appearance of the amide carbonyl band at ν 1,638 cm^{-1} and the shift of the ketone carbonyl band to 1,703 cm^{-1}. The appearance of a band at ν 728 cm^{-1} attributed to C-Cl was also noted, along with the appearance of new bands in CAP in the aliphatic region at ν 12,954 cm^{-1}. The infrared spectrum of CAP-Te-CN was characterized by the disappearance of the C-Cl band and the appearance of a band at ν 2,142 cm^{-1} attributed to the cyanide group .a band appeared at ν47 5 cm^{-1} attributed to C-Te, in addition to shifts in the ketone and amide carbonyl bands. As for the spectra of CAP-Te-X_3 compounds, they were also characterized by the disappearance of the cyanide band, with the remaining bands of the C-Te group at ν (514, 504, 510) cm^{-1}, respectively.

Table 2 FT-IR spectrums of prepared compounds.

	Compound	NH	CH AR	CH alph	C≡N	C=O ketone	C=O amide	C=C	C-N	C-Te	C-Cl
1	ABP	3,338	3,079	---	---	1,635	---	1,589	1,316	---	---
2	CAP	3,350	3,087	2,954	---	1,703	1,638	1,596	1,316	----	728
3	CAP-Te-CN	3,284	3,098	2,959	2,142	1,677	1,655	1,590	1,316	475	---
4	CAP-Te-Cl_3	3,294	3,056	2,928	---	1,653	-	1,594	1,318	514	---
5	CAP-Te-Br_3	3,264	3,118	2,982	---	1,670	1,651	1,597	1,311	504	---
6	CAP-Te-I_3	3,285	3,053	2,927	---	1,654	1,637	1,593	1,317	510	---

NMR spectra

The ^{1}H-NMR spectra of the prepared compounds (400MHz/ DMSO-d_6) showed a set of characteristic signals of substituted proton groups with characteristic shifts and dissociations due to the effect of the relatively large size of the tellurium. The **Table 3** below and The **Figures 3 - 7** show the structural formulas of the prepared compounds and the ^{1}H NMR signals measured for each compound. the most important structures of the prepared compounds and the most important signals appearing for each compound.

As such as the and ^{13}C NMR of prepared compounds showed signals of carbon atoms at characteristic position The **Table 4** below and the **Figures 8 - 12** show the structural formulas of the prepared compounds and the ^{13}C NMR signals measured for each compound. The most important structures of the prepared compounds and the most important signals appearing for each compound.

Table 3 ^{1}H NMR spectrum of prepared compounds.

Symbol	Structural formulas	^{1}H NMR
CAP	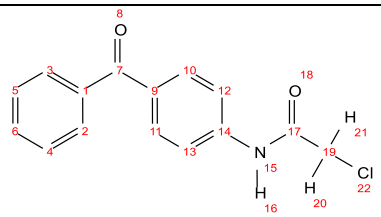	H_{20}, H_{21}(4.33 ppm, s,2H), Ar-H (7.53 - 781 ppm, m, 9H), H_{16} (10.71 ppm, s,1H).
CAP-Te-CN	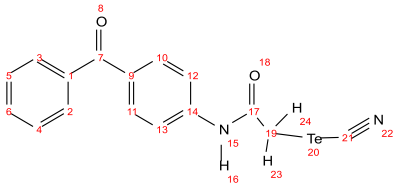	H_{24} (3.72 ppm, s, 1H), H_{23} (4.14 ppm, s, 1H), Ar-H (7.51 - 7.95 ppm, m, 9H), H_{16} (46 ppm, 11.39 ppm, d, 1H).
CAP-Te-Cl_3	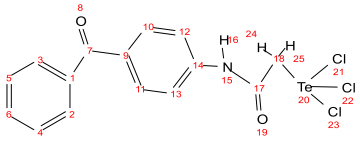	H_{24}, H_{25} (3.60 ppm, s, 2H), Ar-H (7.52 - 7.78 ppm, m, 9H), H_{16} (10.57 ppm, s, 1H).
CAP-Te-Br_3	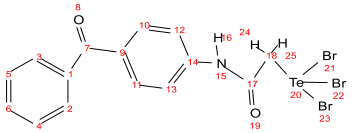	H_{24}, H_{25} (4.11 ppm, s, 2H), Ar-H (7.54 - 7.92 ppm, m, 9H), H_{16} (10.82 ppm, s, 1H).
CAP-Te-I_3	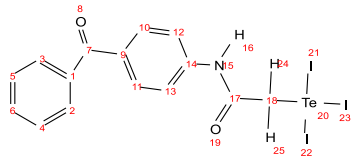	H_{25} (3.40 ppm, s,1H), H_{24} (3.72 ppm, s, 1H), Ar-H (7.51 - 7.75 ppm, m, 9H), H_{16} (10.93 ppm, s, 1H).

Table 4 ^{13}C NMR spectrum of prepared compounds.

Symbol	Structural formulas	^{13}C NMR
CAP	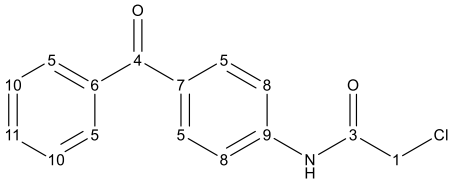	C_1 = 44.10, C_2 = X, C_6 =137.89, C_7 = 132.77, C_9 = 143.04, C_3 = 16,571, C_4= 195.01, C_5 = 131.67, C_{11} = 129.88, C_8 = 119.11, C_{10} = 128.95
CAP-Te-CN	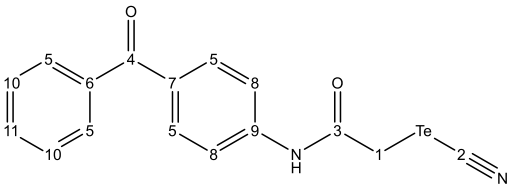	C_1 = 7.69, C_2 = 118.71, C_6, C_7 = 138.01, C_9 = 143.89, C_3 = 172.44, C_4 = 194.68, C_5 = 131.68, C_{11} = 132.70, C_8 = 128.94, C_{10} = 129.86
CAP-Te-Cl_3	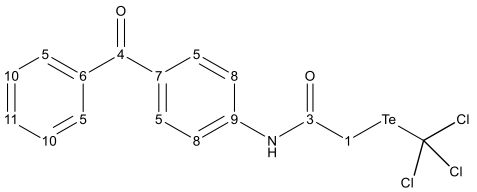	C_1 = 24.68, C_2 = X, C_6 = 137.89, C_7 = 132.72, C_9 = 142.83, C_3 = 165.76, C_4 = 195.07, C_5 = 131.66, C_{11} = 129.86, C_8 = 119.33, C_{10} = 128.93
CAP-Te-Br_3	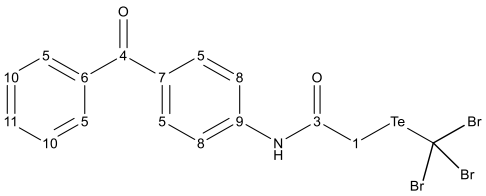	C_1 = 30.79, C_2 = X, C_6 = 137.87, C_7 = 132.82, C_9 = 143.16, C_3 = 165.92, C_4 = 195.03, C_5 = 131.70, C_{11} = 129.90, C_8 = 119.29, C_{10} = 128.98
CAP-Te-I_3	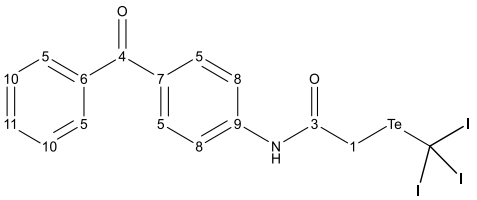	C_1 = 48.45, C_2 = X, C_6 = 137.72, C_7 = 132.82, C_9 = 142.22, C_3 = 163.27, C_4 = 195.02, C_5 = 131.78, C_{11} = 129.91, C_8 = 119.31, C_{10} = 128.98

Mass spectra

The mass spectrum was used to characterize the prepared compounds and confirm their proposed identities by determining their molecular weights and the molecular weights of their ionization fragments. The mass spectrum of the compound CAP showed a set of distinctive peaks. listed below : 273. 72 m/ z due to $[C_{15}H_{12}ClNO_2]^+$ molecular ion, 196. 23 m/ z due to $[C_{13}H_{10}NO]^{\bullet+}$ base beak, 238. 09 m/ z due to $[C_{15}H_{12}NO_2]^{\bullet+}$, 224. 24 m/ z due to $[C_{14}H_{10}NO_2]^{\bullet+}$, 181. 21 m/ z due to $[C_{13}H_9O]^{\bullet+}$,77. 49 mz due to $[C_2H_2ClO]^{\bullet+}$, 105. 12 m/z due to $[C_7H_5O]^{\bullet+}$, 92. 50 m/z due to $[C_2H_3ClNO]^{\bullet+}$, 168. 60 m/z due to $[C_8H_7ClNO]^{\bullet+}$, 77. 11 m/ z due to $[C_6H_5]^{\bullet+}$, 196. 61 m/ z due to $[C_9H_7ClNO_2]^{\bullet+}$, 162. 17 m/z due to $[C_9H_8NO_2]^{\bullet+}$, 134. 16 m/z due to $[C_8H_8NO]^{\bullet+}$, 148. 14 m/z due to $[C_8H_6NO_2]^{\bullet+}$, 120. 13 m/ z due to $[C_7H_6NO]^{\bullet+}$, 120. 13 m/ z due to $[C_7H_6NO]^{\bullet+}$, 65. 10 m/z due to $[C_5H_5]^{\bullet+}$, 53. 08 m/z due to $[C_5H_4]^{\bullet+}$.See **Figure 13** the attached table.

The mass spectrum of the compound CAP-Te-CN showed a set of distinctive peaks. Listed below: 394. 00 m/ z due to $[C_{16}H_{12}N_2O_2Te]^+$ molecular ion, 77. 11 m/ z due to $[C_6H_5]^{\bullet+}$ base beak, 367. 99 m/ z due to $[C_{15}H_{12}NO_2Te]^{\bullet+}$, 238. 27 m/ z due to $[C_{15}H_{12}NO_2]^{\bullet+}$, 155. 91 m/ z due to $[CNTe]^{\bullet+}$, 224. 24 m/ z due to $[C_{14}H_{10}NO_2]^{\bullet+}$, 169. 92 m/ z due to $[C_2H_2NTe]^{\bullet+}$, 196. 23m/ z due to $[C_{13}H_{10}NO]^{\bullet+}$, 197. 92 m/ z due to $[C_3H_2NOTe]^{\bullet+}$, 181. 21m/ z due to $[C_{13}H_9O]^{\bullet+}$, 212. 93 m/ z due to $[C_3H_3N_2OTe]^{\bullet+}$, 288. 96 m/ z due to $[C_9H_7N_2OTe]^{\bullet+}$, 105. 12 m/ z due to $[C_7H_5O]^{\bullet+}$, 316. 96 m/z due to $[C_{10}H_7N_2O_2Te]^{\bullet+}$, 65. 10 m/z due to $[C_5H_5]^{\bullet+}$, 53. 08 m/ z due to $[C_4H_5]^{\bullet+}$, 162. 17 m/ z due to $[C_9H_8NO_2]^{\bullet+}$, 291. 96 m/ z due to $[C9H8NO2Te]^{\bullet+}$, 148. 14 m/ z due to $[C_8H_6NO_2]^{\bullet+}$, 120. 13 m/ z due to

$[C_7H_6NO]^{\bullet+}$, 264.97 m/z due to $[C_8H_9NOTe]^{\bullet+}$, 134.16 m/z due to $[C_8H_8NO]^{\bullet+}$, 120.13 m/z due to $[C_7H_6NO]^{\bullet+}$, 92.12 m/z due to $[C_6H_6N]^{\bullet+}$, 172.92 m/z due to $[C_2H_3OTe]^{\bullet+}$, 187.94m/z due to $[C_2H_4NOTe]^{\bullet+}$, 144.93 /z due to $[CH_3Te]^{\bullet+}$, 130.91 /z due to $[HTe]^{\bullet+}$. See **Figure 14** the attached table.

The mass spectrum of the compound CAP-Te-Cl_3 showed a set of distinctive peaks. listed below:472.90 m/z due to $[C_{15}H_{12}Cl_3NO_2Te]^+$ molecular ion, 77.11 m/z due to $[C_6H_5]^{\bullet+}$ base beak, 291.83 m/z due to $[C_2H_3Cl_3NOTe]^{\bullet+}$, 181.21 m/z due to $[C_{13}H_9O]^{\bullet+}$, 276.82 m/z due to $[C_2H_2Cl_3OTe]^{\bullet+}$, 361.90 m/z due to $[C_9H_8Cl_2NO_2Te]^{\bullet+}$, 332.66 m/z due to $[C_8H_8Cl_2NOTe]^{\bullet+}$, 105.12 m/z due to $[C_7H_5O]^{\bullet+}$, 256.56 m/z due to $[C_2H_4Cl_2NOTe]^{\bullet+}$,241.54 m/z due to $[C_2H_3Cl_2OTe]^{\bullet+}$, 196.23 m/z due to $[C_{13}H_{10}NO]^{\bullet+}$, 224.24 m/z due to $[C_{14}H_{10}NO_2]^{\bullet+}$, 199.51 m/z due to $[Cl_2HTe]^{\bullet+}$, 221.90 m/z due to $[C_2H_3ClNOTe]^{\bullet+}$, 164.88 m/z due to $[ClTe]^{\bullet+}$. See **Figure 15** the attached table.

The mass spectrum of the compound CAP-Te-Br_3 showed a set of distinctive peaks. Listed below:605.58 m/z due to $[C_{15}H_{12}Br_3NO_2Te]^+$molecular ion, 3.18 m/z due to $[CH_2Br_2NTe]^{\bullet+}$ 500.46 m/z due to $[C_8H_7Br_3NOTe]^{\bullet+}$, 105.12 m/z due to $[C_7H_5O]^{\bullet+}$, 181.21 m/z due to $[C_{13}H_9O]^{\bullet+}$, 409.35 m/z due to $[C_2H_2Br_3OTe]^{\bullet+}$, 196.08 m/z due to $[C_{13}H_{10}NO]^{\bullet+}$, 380.68 m/z due to $[CH_2Br_3Te]^{\bullet+}$, 366.66 m/z due to $[Br_3Te]^{\bullet+}$, 449.58 m/z due to $[C_9H_8Br_2NO_2Te]^{\bullet+}$, 77.04 m/z due to $[C_6H_5]^{\bullet+}$, 345.47 m/z due to $[C_2H_4Br_2NOTe]^{\bullet+}$, 302.44 m/z due to $[CH_3Br_2Te]^{\bullet+}$, 445.77 m/z due to $[C_{15}H_{12}BrNO_2Te]^{\bullet+}$, 341.88 m/z due to $[C_8H_7BrNOTe]^{\bullet+}$, 265.85m/z due to $[C_2H_3BrNOTe]^{\bullet+}$, 249.54 m/z due to $[C_2H_2BrOTe]^{\bullet+}$, 222.84 m/z due to $[CH_2BrTe]^{\bullet+}$, 208.82 m/z due to $[BrTe]^{\bullet+}$, 130.91 m/z due to $[HTe]^{\bullet+}$. See **Figure 16** the attached table.

The mass spectrum of the compound CAP-Te-I_3 showed a set of distinctive peaks. listed below:746.58 m/z due to $[C_{15}H_{12}I_3NO_2Te]^+$ molecular ion, 254.50 m/z due to $[ITe]^{\bullet+}$ base peak, 510.62 m/z due to $[I_3Te]^{\bullet+}$, 74.441m/z due to $[C_2H_4I_2NOTe]^{\bullet+}$,181.21 m/z due to $[C_{13}H_9O]^{\bullet+}$, 424.45 m/z due to $[C_2H_3I_2OTe]^{\bullet+}$, 196.23 m/z due to $[C_{13}H_{10}NO]^{\bullet+}$, 224.24 m/z due to $[C_{14}H_{10}NO_2]^{\bullet+}$, 382.42 m/z due to $[HI_2Te]^{\bullet+}$, 387.65 m/z due to $[C_8H_7INOTe]^{\bullet+}$, 105.12 m/z due to $[C_7H_5O]^{\bullet+}$, 298.82 m/z due to $[C_2H_2IOTe]^{\bullet+}$, 268.53 m/z due to $[CH_2ITe]^{\bullet+}$. See **Figure 17** the attached table.

Results of cyclic voltammetry (CV)

The compound CAP showed 2 reduction peaks at –1.25 and –1.7 mV and 1 oxidation peak at 1.84 mV. The compound CAP-Te-CN showed 3 reduction peaks at –0.99, –1.35, and –1.55 mV and 3 oxidation peaks at –0.14, –1.44, and 0.83 mV. CAP-Te-Br3 showed 4 reduction peaks at –1.19, –1.48, –1.78, and 0.49 mV and 3 oxidation peaks at –1.72, 0.19, and 1.01 mV. The compound CAP-Te-Cl3 showed 3 reduction peaks at –0.7, –1.03, and –1.82 mV and 3 oxidation peaks at –1.06, –0.11, and 1.51 mV, whereas the compound CAP-Te-I3 showed 3 reduction peaks at –0.94, –1.41, and –1.63 mV and 3 oxidation peaks at 1.21, 1.53, and 0.65 mV.

Table 5 Cyclic voltammetry measurements.

Compound	Ep^c	Ip^c	FIp^c	Ep^a	Ip^a	FIp^a	ΔE	E°	Ipa/Ipc
CAP	–1.25	17.65	55.85	--	--	--	3.18	–0.11	1.22
	–1.70	25.88	81.89	--	--	--			
	--	--	--	1.48	31.58	57.65			
CAP-Te-Br3	–1.19	–27.62	87.40	–1.72	–6.02	10.99	2.79	–0.385	0.35
	–1.48	–39.91	126.29	-0.19	5.39	9.84			
	–1.78	–51.69	163.57	--	--	--			
	0.49	–11.67	36.93	1.01	18.41	33.61			
CAP-Te-Cl3	–0.70	–11.71	37.05	–1.06	1.66	3.03	3.33	–0.155	1.02
	–1.03	–16.57	52.43	–0.11	7.81	14.25			
	–1.82	–38.79	122.75	--	--	--			
	--	--	--	1.51	39.61	72.32			

Compound	Ep^c	Ip^c	FIp^c	Ep^a	Ip^a	FIp^a	ΔE	E°	Ipa/Ipc
CAP-Te-CN	–0.99	–22.58	71.45	–1.13	3.10	5.66	2.87	–0.425	0.48
	–1.64	–73.39	232.24	–0.14	17.86	32.60			
	–1.86	–79.85	252.68	--	--	--			
	0.76	–5.36	16.96	1.01	38.89	71.00			
CAP-Te-I3	–0.94	19.37	61.29	10.21	6.99	12.76	2.66 1.17	–0.17 0.135	1.58 1.97
	–1.41	21.93	69.39	--	--	--			
	–1.63	37.12	117.46	--	--	--			
	--	--	--	1.53	47.74	87.16			
	--	--	--	0.65	10.88	19.86			

The compound showed the lowest reduction potential at -1.86 mV; therefore, it has the lowest electron density, and hence it will require the minimum potential to achieve electron gain. The compound CAP-$TeBr_3$ has shown the lowest oxidation potential at –1.72; hence, with an increase in electron density, electron loss will be made easy. While the energy difference values show the stability of the intermediate state during the chemical reaction, the compound CAP-Te-Cl_3 proved to have the highest degree of electrochemical stability, amounting to $\Delta E = 3.33$, while the least electrochemically stable intermediate state was observed in the compound CAP-Te-I_3, having $\Delta E = 2.66$. See more in **Table 5** and **Figures 18** - **24**.

Results of molecular docking

Molecular docking is the key tool of the drug discovery pipeline. The present study made all molecular docking calculations on MOE software to predict the binding mode of the prepared compounds (A, B, C and D) with the protein N-domain of GRP94 bound to the HSP90 inhibitor PU-H54 (3O2F). The binding affinities and features of the investigated compounds (A, B, C and D) towards 4XEM are listed in **Tables 6** and **7** shows the best binding poses of compounds (A, B, C and D) against target proteins.

The figures and tables below show the 2D and 3D representations of interactions of the examined compounds with the important amino acid residues of 3O2F protein. Compounds (A, B, C, and D) have demonstrated good binding affinity values with the protein (PDB ID: 3O2F) as elaborated in **Tables 6** and **8**. The binding and mode of interactions of the compound (A, B, C and D) with (PDB ID: 3O2F) protein is shown in 2D and 3D figures. From the interactions, it has been showed that primarily there are different types of interactions (hydrogen bonding and hydrophobic interactions). Interactions were further examined for bond lengths and hydrogen bonds in the active site and were illustrated in the last figures. Results from these figures indicated that compounds (A, B, C and D) form interactions with three different amino acid residues: One as an H-donor, another as an H-acceptor, and the other as H-pi; one more H-acceptor and pi-H, with water and amino acids. The distance and energy binding of interaction are listed in **Tables 6** and **8**.

Molecular docking analysis results

The molecular docking analysis of compounds A1 to D3 revealed important insights regarding their binding affinities, modes of interaction, and binding stability with the target protein. Among all tested ligands, compound D1 demonstrated the highest binding affinity with a score of -7.68717 kcal/mol, followed closely by D2 (-7.42544 kcal/mol) and A1 (-7.31744 kcal/mol). These negative values reflect stronger and more favorable binding interactions.

Additionally, Root Mean Square Deviation (RMSD) values, which indicate the stability and reliability of the binding pose, were acceptable across most compounds. Notably, D2 exhibited the lowest RMSD (1.070012 Å), suggesting a stable and well-fitted docking conformation. In contrast, compounds like B1 and D3 had slightly higher RMSD values (2.91 Å and 2.53 Å, respectively), which may indicate greater flexibility or less optimal fitting in the binding pocket. Several types of interactions contributed to binding stabilization, including hydrogen bonds (H-donor and

H-acceptor), pi-H stacking, ionic interactions, and pi-pi interactions. For instance: Compound C1 displayed a particularly strong hydrogen bond with GLU 158, with an interaction energy of -15.3 kcal/mol, highlighting a significant electrostatic attraction. Compound A3 formed multiple interactions (H-donor, H-acceptor, and ionic) with residues MET 154, ASP 110, HOH 441, and LYS 114, supporting a multivalent binding profile. D1 and D2 formed combined interactions such as H-acceptor, H- donor, and pi- pi stacking with critical residues like ASN 162, GLU 158, MET 154, and PHE 195, strengthening their docking scores. These interactions not only help stabilize the ligand within the binding pocket but also suggest that these compounds could exhibit effective bioactivity in a biological context. Moreover, recurring interaction with key residues such as ASN 107, ASP 110, and GLY 153 across several ligands implies the importance of these residues in anchoring small molecules.

In summary, the docking results highlight D1 as the most promising candidate, considering both its binding affinity and interaction profile. However, compounds A1, D2, and C1 also exhibited strong potentials and may warrant further *in vitro* or *in silico* validation. The diversity of interactions (e.g., hydrogen bonds and pi- stacking) across ligands suggests that rational design strategies may further optimize these scaffolds for enhanced affinity and selectivity

Computational analysis

Through the mathematical relations as in the Eqs. (1) - (4).

$$\mu = \left(\frac{\delta E}{\delta N}\right)_{V(r^{\rightarrow}),T} \quad (1)$$

$$\eta = \frac{1}{2}\left(\frac{\delta^2 E}{\delta N^2}\right)_{V(r^{\rightarrow}),T} \quad (2)$$

$$\delta = \frac{1}{2\eta} \quad (3)$$

$$\omega = \frac{\mu^2}{2\eta} \quad (4)$$

The text discusses key concepts in chemical potential and reactivity, including μ (chemical potential), η (chemical hardness), S (chemical softness), and ω (electrophilicity). These global quantities are derived from the total electron energy (E), the number of electrons (N), and the external potential (V(r→)). The calculations for these properties utilize two approaches, with the first being a finite difference approximation that assesses changes in total electronic energy when electrons are added or removed from a neutral molecule. Additionally, the differences in the energies of the highest occupied molecular orbital (HOMO) and the lowest unoccupied molecular orbital (LUMO) are foundational to Koopman's theory, which underpins the understanding of molecular reactivity [47,50,51] . Global quantities that are derivable from Eqs. (5) - (6) are approximated using finite differences.

$$x = \frac{(IP+EA)}{2} \quad (5)$$

$$\eta = \frac{(IP-EA)}{2} \quad (6)$$

The equilibrium geometries for all CT (charge-transfer) complex compounds in the gaseous phase were carefully tuned at theory (DFT) [49] using the functional of a (B3LYP,) in (G09W) and the basis standard established (3-21G) see **Tables 11 -13**. The energies of (HOMO) High Occupied Molecular Orbital and (LUMO) Low Unoccupied Molecular Orbital are the states of electrons, defining certain regions where atomic and molecular orbitals combine linearly, leading to the existence of electrons with quantized energy. The relationship between the energy band gap (Eg) Eq. (7) and the difference in (LUMO) and (HOMO) [52]. The property of the Eg is essential in solids because it makes material prediction possible, if it is an insulator, semiconductor, or conductor. It depicts the difference in energy between the higher full energy level and the lower level of virtual energy [53]. See **Table 11**.

$$E_g = E_{LUMO} - E_{HOMO} \quad (7)$$

Electronegativity and electrophilicity

The molecule' s ability to take up electrons is measured by chemical electrophilicity, which is determined by chemical electrophilicity, which is dependent on chemical hardness and chemical potential, where hardness is resistance to deformation and change. On the other hand, electronegativity measures an atom's capacity to attract an electron density (a shared pair of electrons) towards itself. Calculating electrophilicity

and electronegativity can be done using relationships in Eqs. (8) - (9). [47,48]; see **Table 12**.

$$x = \frac{(E_{HOMO}+E_{LUMO})}{2} \quad (8)$$

$$\omega = \frac{x^2}{2\eta} \quad (9)$$

Ionization potential and electron affinity

Measurement of the bond's strength is done via the ionization potential among an atom and an electron. It possesses the same amount of energy as what is needed to expel one electron from a neutral atom the gap phase. When an atom takes an electron, energy is released, which is referred to as having "electron affinity". It is the necessary energy to remove electron from a negatively charged ion. This is consistent with Koopman's theory [45], as seen in Eqs. (10) - (11) and **Table 13**.

$$I.P = -E_{HOMO} \quad (10)$$

$$E.A = -E_{LUMO} \quad (11)$$

HSAB Principle (Acid Base Hardness Softness)

When utilized as acids and bases in chemistry, this principle describes how atoms or molecules behave. First, it must be shown that soft and hard acids are acceptors, whereas hard and soft bases are donors. Eqs. (12) and (13) are used to show both hardness and softness [54-57].

$$\eta = \frac{(IP-EA)}{2} \quad (12)$$

$$\delta = \frac{1}{2\eta} \quad (13)$$

Table 6 The binding affinity and rmsd result of 3O2f protein from docking process.

Compounds	mseq	Binding affinity	Rmsd(Å)	E_conf	E_place	E_score1	E_refine	E_score2
A1	1	–7.31744	2.416457	–76.9436	–66.1698	–10.3304	–41.0143	–7.31744
A2	1	–6.31382	1.18306	–58.4218	–54.4347	–10.1763	–27.3708	–6.31382
A3	1	–6.00138	1.788493	–47.6585	–64.6519	–9.87096	263.6569	19.00138
B1	2	–6.91145	2.915595	–84.2466	–74.1589	–9.96447	–39.32	–6.91145
B2	2	–6.12775	1.932813	–66.8673	–55.2534	–9.80327	–27.5167	–6.12775
B3	2	–5.31393	1.059629	–62.7339	–77.2809	–9.97388	–4.59295	–5.31393
C1	3	–6.90572	1.196662	–43.4447	–65.6351	–9.87692	–37.5196	–6.90572
C2	3	–6.89822	2.222129	–41.552	–81.6302	–9.45598	–36.7182	–6.89822
C3	3	–6.6666	1.765592	–41.2078	–66.2424	–9.31246	–37.292	–6.6666
D1	4	–7.68717	2.019911	–66.9421	–81.3093	–10.299	–44.5309	–7.68717
D2	4	–7.42544	1.070012	–60.0649	–68.9911	–11.089	–28.3692	–7.42544
D3	4	–6.88729	2.539685	–61.8727	–74.4985	–10.2554	–33.7197	–6.88729

Table 7 The compound's smiles.

Compounds	Smile
A1	[Te](Br)(Br)(Br)#CC(=O)Nc1ccc(C(=O)c2ccccc2)cc1
A2	[Te](Br)(Br)(Br)#CC(=O)Nc1ccc(C(=O)c2ccccc2)cc1
A3	[Te](Br)(Br)(Br)#CC(=O)Nc1ccc(C(=O)c2ccccc2)cc1
B1	[Te](Cl)(Cl)(Cl)#CC(=O)Nc1ccc(C(=O)c2ccccc2)cc1
B2	[Te](Cl)(Cl)(Cl)#CC(=O)Nc1ccc(C(=O)c2ccccc2)cc1

Compounds	Smile
B3	[Te](Cl)(Cl)(Cl)#CC(=O)Nc1ccc(C(=O)c2ccccc2)cc1
C1	[Te](C#N)CC(=O)Nc1ccc(C(=O)c2ccccc2)cc1
C2	[Te](C#N)CC(=O)Nc1ccc(C(=O)c2ccccc2)cc1
C3	[Te](C#N)CC(=O)Nc1ccc(C(=O)c2ccccc2)cc1
D1	I[Te](I)(I)#CC(=O)Nc1ccc(C(=O)c2ccccc2)cc1
D2	I[Te](I)(I)#CC(=O)Nc1ccc(C(=O)c2ccccc2)cc1
D3	I[Te](I)(I)#CC(=O)Nc1ccc(C(=O)c2ccccc2)cc1

Table 8 Details of the best poses of protein $3O_2F$

Compound	Binding Affinity Kcal/mol	Rmsd (Å)	Atom of compound	Atom of Receptor	Involved receptor residues	Type of interaction bond	Distance (Å)	E (kcal/mol)
A1	–7.31744	2.41645	BR 30	ND2	ASN 107	(A) H-acceptor	3.46	–0.7
A2	–6.31382	1.18306	6-ring	CD	LYS 114	(A) pi-H	4.38	–0.6
A3	–6.00138	1.78849	N 24	SD	MET 154	(A) H-donor	3.84	–1.2
			BR 30	OD2	ASP 110	(A) H-donor	2.70	–3.0
			O 13	O	HOH 441	(A) H-acceptor	2.79	–1.5
			C 28	NZ	LYS 114	(A) ionic	3.97	–0.6
B1	–6.91145	2.91559	CL 30	ND2	ASN 107	(A) H-acceptor	3.48	–0.7
B2	–6.12775	1.93281	CL 32	O	HOH 441	(A) H-acceptor	2.58	–0.5
B3	–5.31393	1.05962	CL 30	O	GLY 153	(A) H-donor	3.11	–1.2
			CL 31	O	HOH 362	(A) H-acceptor	2.52	–0.2
C1	–6.90572	1.19666	TE 31	O	GL 153	(A) H-donor	3.43	–3.8
			TE 31	OE1	GLU 158	(A) H-donor	3.41	–15.3
			N 33	NZ	LYS 114	(A) H-acceptor	3.01	–7.5
C2	–6.89822	2.22212	TE 31	OD2	ASP 110	(A) H-donor	4.40	–0.6
			O 13	ND2	ASN 107	(A) H-acceptor	2.92	–3.0
			N 33	NZ	LYS 114	(A) H-acceptor	3.28	–1.7
C3	–6.6666	1.76559	TE 31	O	GLY 153	(A) H-donor	3.72	–2.9
			N 33	NZ	LYS 114	(A) H-acceptor	3.34	–1.9
			6-ring	CA	PHE 199	(A) pi-H	4.24	–0.6
D1	–7.68717	2.01991	I 32	ND2	ASN 162	(A) H-acceptor	4.15	–0.6
			TE 29	OE1	GLU 158	(A) ionic	3.34	–2.6
D2	–7.42544	1.07001	I 32	O	PHE 195	(A) H-donor	3.52	–2.8
			6-ring	CE	MET 154	(A) pi-H	4.22	–0.6
D3	–6.88729	2.53968	I 31	ND2	ASN 107	(A) H-acceptor	3.44	–0.8
			6-ring	6-ring	PHE 195	(A) pi-pi	3.86	

Table 11 Shows the shows the electronic state of organochalcanids compounds.

Compound	HOMO ev	LUMO ev	ΔE_{gap}
CAP	–6.368462	–2.269941	4.098521
CAP-Te-CN	–5.29852	–2.200825	3.097695
CAP-Te-Cl_3	–1.65851	–1.101773	0.556737
CAP-Te-Br_3	–1.39048	–0.842724	0.547756
CAP-Te-I_3	–1.86177	–1.352114	0.509656

Computational study of organoselenium compounds and their derivatives

The Computational study of Tullerocyanates and their trihalide derivatives CAP-Te-CN, (CAP-Te-X_3) where (X= Cl, Br, I) Also the same computational analyses are applied on of reduction compounds. In the present study, a comparison of the HOMO energies for Reduction and nonreduction of compounds and their derivatives, is presented in **Table 11** to find out that the HOMO energy of CAP-Te-Br_3 compound is greater than others compounds. This is due to the strength and stability of CAP-Te-Br_3. A general rule of thumb is that the greater the HOMO-LUMO gap, the compound more stable. In addition to the HOMO representing electron donors, its energy is attached to three atoms of Br bonded to the Tellurium atom. Whereas the lowest in HOMO energy was compound CAP. In LUMO energy is as follows: CAP-Te-Br_3 > of others. As a result, can help predict where addition to pi ligands will occur [58,59]. As shown in **Tables 11**, **12** and **13**.

In **Table 12**, the electronegativity of CAP-Te-Br_3 was larger than the electronegativity of the others. It is clear that compound CAP-Se-Cl_3 is the most reactive while compound CAP is the least reactive of all. The electronegativity (χ) is a measure of the attraction of an atom for electrons in a covalent bond; thus, compound CAP-Te-Br_3 it does exhibit high charge flow. Also, the obtained results show that compound CAP-Te-Br_3 is strongly electrophilic, while compound CAP is nucleophilic. The CAP-Te-I_3 compound was the larger Electrophilicity, whereas CAP-Te-Br_3 has the least electrophilicity among all prepared compounds for the same reason above [60-62].

Table 12 Electronegativity and electrophilicity of compounds.

Compound	Electronegativity X (eV)	Electrophilicity W (eV)
CAP	-4.3192015	4.551764
CAP-Te-CN	-3.74967	4.538866
CAP-Te-Cl_3	-1.3801415	3.4213471
CAP-Te-Br_3	-1.116602	2.2761960
CAP-Te-I_3	-1.606942	5.0666775

According to **Table 13**, the Compounds can be classified as donors or acceptors through a comparison between them. The hardness of CAP is greater than the hardness of the others compounds hence CAP will behave as a hard base. The softness of CAP-Te-I_3 was greater than of the others compounds, indicating that CAP-Te-I_3 will behave as a soft base [61,63].

Table 13 Ionization potential, electron affinity, softness, and hardness for organochalconids.

Compound	Ionization potential (I.P)(eV)	Electron affinity (E.A)(eV)	Hardness(η)	Softness(δ)
CAP	6.368462	2.269941	2.049260	0.24399045
CAP-Te-CN	5.29852	2.200825	1.548847	0.3228206
CAP-Te-Cl_3	1.65851	1.101773	0.278368	1.7961802
CAP-Te-Br_3	1.39048	0.842724	0.273878	1.8256303
CAP-Te-I_3	1.86177	1.352114	0.254828	1.9621077

Conclusions

This study presents straightforward methods for synthesizing new organotellurium compounds, achieving yields between 33 and 87% . The characterization of these compounds was confirmed through Fourier transform infrared spectroscopy and single- hydrogen NMR, aligning with previous research findings. Cyclic voltammetry revealed that the reactions were irreversible, with varying redox potentials indicating differences in reaction stability and intermediate behavior. Additionally, molecular docking studies suggest the compounds have potential as anticancer agents, with density functional theory (DFT) employed to optimize their geometry and electronic properties, demonstrating high stability and effective interactions within the donor-acceptor systems.

Acknowledgements

I would like to extend my thanks and gratitude to all the faculty members in the Chemistry Department / College of Science / University of Thi Qar.

Declaration of Generative AI in Scientific Writing

The authors confirm the use of generative AI tools, such as QuillBot and OpenAI's ChatGPT, during the preparation of this manuscript. These tools were employed solely for language editing and grammar correction and were not used for content generation or data interpretation. The authors assume full responsibility for the accuracy, integrity, and conclusions presented in this work.

CRediT Author Statement

Ahmed Mohammed AlSanafi: contributed to the conceptualization, methodology, investigation, formal analysis, and writing of the original draft.

Nuha Hussain Al-Saadawy: assisted in validation, data curation, computational studies, and writing—review and editing. Specifically, **Ahmed Mohammed AlSanafi** performed the synthesis, characterization, and cyclic voltammetry (CV) experiments, while **Nuha Hussain Al-Saadawy** conducted the theoretical molecular docking against breast cancer and computational studies to determine the energy gap and reviewed and approved the final manuscript.

References

[1] C Niu, G Qiu, Y Wang, P Tan, M Wang, J Jian, H Wang, W Wu and PD Ye. Tunable chirality-dependent nonlinear electrical responses in 2D tellurium. *Nano Letters* 2023; **23(18)**, 8445-8453.

[2] J Hader, SC Liebscher, JV Moloney and SW Koch. Microscopic analysis of linear and nonlinear electro-optical properties of tellurium. Nonlinear Frequency Generation and Conversion: Materials and Devices XXII. *In*: Proceedings of the SPIE LASE Conference, San Francisco, California. 2023, p. 124050D.

[3] A Das and BK Banik. Semiconductor characteristics of tellurium and its implementations. *Physical Sciences Reviews* 2023; **8(12)**, 4659-4687.

[4] B Huang, Z Lei, X Cao, A Wei, L Tao, Y Yang, J Liu, Z Zheng and Y Zhao. High-quality two-dimensional tellurium flakes grown by high-temperature vapor deposition. *Journal of Materials Chemistry C* 2021; **9(40)**, 14394-14400.

[5] AH Sheaa, AA Al-Fregi, and HK Mousa. Convenient methods for the synthesis organotellurium compounds derived from pyrazole derivatives: Synthesis and antimicrobial evaluation. *Phosphorus, Sulfur, and Silicon and the Related Elements* 2022; **197(8)**, 867-875.

[6] YS Panwar, M Aynyas, J Pataiya and SP Sanyal. Structural and electronic properties of thulium compounds. *Journal of Metastable and Nanocrystalline Materials* 2017; **28**, 59-64.

[7] AJ Scheen. Dulaglutide (Trulicity®) : A new once-weekly agonist of glucagon-like peptide-1 receptors for type 2 diabetes. *Revue Médicale de Liège* 2016; **71(3)**, 154-160.

[8] M Hanias, A Anagnostopoulos, K Kambas and J Spyridelis. On the non-linear properties of $TlInX_2$ (X = S, Se, Te) ternary compounds. *Physica B: Condensed Matter* 1989; **160(2)**, 154-160.

[9] DMA Murad, AZ Al-Rubaie and AA Al-Najar. Conductametric studies of some organotellurium (IV) trihalides. *Journal of Physics Conference Series* 2019; **1279**, 012079.

[10] J Pietikainen, A Maaninen, RS Laitinen and M Nissinen. Novel tellurium halides. *Phosphorus, Sulfur, and Silicon and the Related Elements* 2001; **169(1)**, 129-132.

[11] E Faoro, GM Oliveira and ES Lang. Synthesis and structural characterization of the novel T-shaped Organotellurium (II) Dihalides (PyH) [mesTeClBr] and (PyH) [$mesTeX_2$] (Py = pyridine; mes = mesityl; X = Cl, Br). *Zeitschrift für Anorganische und Allgemeine Chemie* 2006; **632(12-13)**, 2049-2052.

[12] R Kniep and A Rabenau. Subhalides of tellurium: In physical and inorganic chemistry. *Springer* 1983; **111**, 145-192.

[13] WM Ahmed, N Al-Saadawy and MI Abowd. Synthesis and characterization of a new organoselenium and organotellurium compounds depending on 9-chloro-10-nitro-9, 10-dihydroanthracene. *Annals of the Romanian Society for Cell Biology* 2021; **25(4)**, 11035-11043.

[14] A Yousefi and A Caticha. Entropic Density Functional Theory. *Entropy* 2023; **26(1)**, 10.

[15] A Singh, HP Gogoi and P Barman. *Computational chemistry. In*: P Barman and A Singh (Eds.). Schiff base metal complexes: Synthesis and applications. John Wiley & Sons, New Jersey, 2023, p. 113-118.

[16] B Huang, GF Rudorff and OA Lilienfeld. Towards self-driving laboratories: The central role of density functional theory in the AI age. ArXiv preprint 2023. https://arxiv.org/abs/2304.03272

[17] H Jiang and HY Sun. Density-functional theory. Quantum chemistry in the age of machine learning ed. PO Dral, Elsevier, 2023, p. 27-65.

[18] HM Ajeel, ZT Hussain, AHK Elttayef and KM Thajeel. Study of structural, optical and electrical properties of cadmium telluride thin films. *University of Thi-Qar Journal of Science* 2014; **4(4)**, 50-55.

[19] TT Yang and WA Saidi. Simple approach for reconciling cyclic voltammetry with hydrogen adsorption energy for hydrogen evolution exchange current. *The Journal of Physical Chemistry Letters* 2023; **14(18)**, 4164-4171.

[20] Q Song, H Li, J Liu and S Hu. Electrodeposition of Se on carbon-supported Pt nanoparticles by cyclic voltammetry. *Journal of Solid State Electrochemistry* 2021; **25**, 2471-2478.

[21] Y Lin, C Lian, MU Berrueta, H Liu and R Roij. Microscopic model for cyclic voltammetry of porous electrodes. *Physical Review Letters* 2022; **128(20)**, 206001.

[22] K Vaddi and O Wodo. Active knowledge extraction from cyclic voltammetry. *Energies: Open Access Journal of Energy Research, Engineering and Policy* 2022; **15(13)**, 4575.

[23] S Pluczyk, M Vasylieva and P Data. Using cyclic voltammetry, UV-Vis-NIR, and EPR spectroelectrochemistry to analyze organic compounds. *Journal of Visualized Experiments* 2018; **140**, 56656.

[24] A Ali and N Toama. DFT/TD-DFT study of D–π–A dyes explore the NLO properties. *University of Thi-Qar Journal of Science* 2023; **10(1)**, 36-41.

[25] P Uppathi, S Rajakumari and KV Saritha. Molecular docking: An emerging tool for target-based cancer therapy. *Critical Reviews in Oncogenesis* 2025; **30(1)**, 1-13.

[26] Nico Martarelli, M Capurro, G Mansour, RV Jahromi, A Stella, R Rossi, E Longetti, B Bigerna, M Gentili, A Rosseto, R Rossi, C Cencini, C Emiliani, S Martino, M Beeg, M Gobbi, E Tiacci, B Falini, F Morena and VM Perriello. Artificial intelligence-powered molecular docking and steered molecular dynamics for accurate scFv selection of anti-CD30 chimeric antigen receptors. *International Journal of Molecular Sciences* 2024; **25(13)**, 7231.

[27] NK Borah, Y Tripathi, A Tanwar, D Tiwari, A Sinha, S Sharma, N Jabalia, RJ Mani, S Santoshi and H Bansal. *Artificial Intelligence-Powered Molecular Docking: A Promising Tool for Rational Drug Design. In:* A Khanna, M El Barachi, S Jain, M Kumar and A Nayyar (Eds.). Artificial Intelligence and Machine Learning in Drug Design and Development. Wiley & Sons, New Jersey, 2023, p. 157-188.

[28] A Dighe and AE Tajamulhaq. An Overview of Molecular Docking. *Asian Journal of Pharmaceutical Research* 2024; **14(3)**, 336-340.

[29] SK Nayak and B Ray, Molecular Docking: Concept and Application. *Novel Aspects on Pharmaceutical Research* 2023; **1**, 35-48.

[30] E Thejeel and AH Mekky. Synthesis, absorption, distribution, metabolism, excretion, toxicology (ADMET) and molecular docking studies of some pyridin-2 (1H)-one derived from a apocynin in Thi-Qar Governorate. *University of Thi-Qar Journal of Science* 2023; **10(2)**, 73-80.

[31] S Kanwar and S Sharma. Thienopyrimidines as hetryl moiety in 2-azetidinones: Synthesis of 4-hetryl-2-azetidinones. *ChemInform: Selected Abstracts in Chemistry* 2005; **44**, 2367-2371.

[32] R Iwamoto. FT-IR/NIR spectroscopic study of interactions between water and alkylamines. *Bulletin of the Chemical Society of Japan* 2019; **92(6)**, 1117-1126.

[33] JR Sohn and JT Kim. Infrared study of alkyl ketones adsorbed on the interlamellar surface of montmorillonite. *Langmuir: The ACS Journal of Surfaces and Colloids* 2000; **16(12)**, 5430-5434.

[34] A Mukherjee, S Tothadi, S Chakraborty, S Ganguly and GR Desiraju. Synthon identification in co-crystals and polymorphs with IR spectroscopy: Primary amides as a case study. *CrystEngComm* 2013; **15(23)**, 4640-4654.

[35] MR Mucalo, RP Cooney and GA Wright. Fourier-transform infrared studies of the corrosion of nickel in aqueous cyanide media. *Journal of the Chemical Society, Faraday Transactions* 1990; **86(7)**, 1083-1086.

[36] F Cataldo. 13C NMR and FT-IR spectra of thiocyanogen, S2 (CN) 2, selenocyanogen, Se2 (CN) 2, and related compounds. *Polyhedron* 2000; **19(6)**, 681-688.

[37] AM Daoud and HA Mahdi. Synthesis, characterization and evaluation biological activity of new schiff base compounds and their complexes with some transition elements. *University of Thi-Qar Journal of Science* 2017; **6(2)**, 81-90.

[38] DL Joo, DJ Clouthier and R Judge. Experimental proof of the case (ab) coupling hypothesis in the first excited triplet state of selenoformaldehyde (H 2 C= Se). *The Journal of Chemical Physics* 2000; **112(5)**, 2285-2291.

[39] Y Cao, F Lei, Y Li, S Qiu, Yan Wang, W Zhang and Z Zhan. A MOF-derived carbon host associated with Fe and Co single atoms for Li–Se batteries. *Journal of Materials Chemistry A: Materials for Energy and Sustainability* 2021; **9(29)**, 16196-16207.

[40] AK Rashid, RB Yahya and PS Wai. Synthesis of spectral, thermal and electrochemical properties of new thermally stable: Blue light emitting materials based aromatic polyamide. *Asian Journal of Chemistry* 2014; **26(13)**, 3854.

[41] D Leitz, A Virmani, Y Morgenstern, F Zischka and AJ Kornath. Preparation and structure of protonated selenourea. *European Journal of Inorganic Chemistry* 2018; **2018(47)**, 5053-5057.

[42] M Aja, M Jaya , KV Nair and IH Joe. FT-IR spectroscopy as a sentinel technology in earthworm toxicology. *Spectrochimica Acta Part A: Molecular and Biomolecular Spectroscopy* 2014; **120**, 534-541.

[43] LA Naser, AF Nasir and ZM Mahdi. Synthesis, characterization, antimicrobial activity and computational study of new 3-(1-methyl-2-((1E, 2E)-3-phenylallylidene) hydrazinyl)-5-phenyl-4H-1, 2, 4-triazole with some transition metal ions.

University of Thi-Qar Journal of Science 2023; **10(1)**, 144-149.

[44] NG Salih and HR Obayes. Theoretical study of *[*N*]*-Helicene structure *(*N= 6, 12, 18, 24, 30, 36, 42, 48, 54*)* using DFT. *Solid State Technology* 2021; **64(2)**, 3909-3919.

[45] X Wang and TC Berkelbach. Excitons in solids from periodic equation-of-motion coupled-cluster theory. *Journal of Chemical Theory and Computation* 2020; **16(5)**, 3095-3103.

[46] AM Khuodhair, FN Ajeel and MO Oleiwi. Density functional theory investigations for the electronic and vibrational properties of donor-acceptor system. *Journal of Applied Physical Science International* 2016; **6(4)**, 202-209.

[47] RM Kubba and MA Mohammed. Theoretical and experimental study of corrosion behavior of carbon steel surface in 3.5% NaCl and 0.5 M HCl with different concentrations of quinolin-2-one derivative. *Baghdad Science Journal* 2022; **19(1)**, 105-120.

[48] RM Kubba, MA Mohammed and LS Ahamed. *DFT* calculations and experimental study to inhibit carbon steel corrosion in saline solution by quinoline-2-one derivative*:* Carbon steel corrosion. *Baghdad Science Journal* 2021; **18(1)**, 0113.

[49] S Sowlati-Hashjin, M Karttunen and CF Matta. Manipulation of diatomic molecules with oriented external electric fields*:* linear correlations in atomic properties lead to nonlinear molecular responses. *The Journal of Physical Chemistry A* 2020; **124(23)**, 4720-4731.

[50] AS Alwan, SK Ajeel and ML Jabbar. Theoretical study for Coronene and Coronene-Al, B, C, Ga, In and Coronene-O interactions by using density functional theory. *University of Thi-Qar Journal of Science* 2019; **14(4)**, 1-14.

[51] HM El-Lateef, S Shaaban, MM Khalaf, A Toghan and K Shalabi. Synthesis, experimental, and computational studies of water soluble anthranilic organoselenium compounds as safe corrosion inhibitors for J55 pipeline steel in acidic oilfield formation water. *Colloids and Surfaces A: Physicochemical and Engineering Aspects* 2021; **625**, 126894.

[52] S Millefiori and A Alparone. Second hyperpolarisability of furan homologues C_4H_4X *(*X= O, S, Se, Te*):* Ab initio HF and DFT study. *Chemical Physics Letters* 2000; **332(1-2)**, 175-180.

[53] ML Jabbar. Theoretical study for the interactions of Coronene-Y interactions by using Density functional theory with hybrid function. *University of Thi-Qar Journal* 2018; **13(3)**, 28-41.

[54] FH Hanoon, ML Jabbar and AS Alwan. Effect of thickness on the fractal optical modulator for MgF 2, LiF, AL 2 O 3 materials by testing modulation transfer function *(*MTF*)*. *Journal of College of Education for Pure Science* 2017; **7(4)**, 168-182.

[55] V Coropceanu, O Kwon, B Wex, BR Kaafarani, NE Gruhn, JC Durivage, DC Neckers and JL Brédas. Vibronic coupling in organic semiconductors*:* The case of fused polycyclic benzene-thiophene structures. *Chemistry–A European Journal* 2006; **12(7)**, 2073-2080.

[56] H.S Mohammed and NH Al-Saadawy. Synthesis, characterization, and theoretical study of novel charge-transfer complexes derived from 3, 4-selenadiazobenzophenone. *Indonesian Journal of Chemistry* 2022; **22(6)**, 1663-1672.

[57] M Panhans, S Hutsch, J Benduhn, KS Schellhammer, VC Nikolis, T Vangerven, K Vandewal and F Ortmann. Molecular vibrations reduce the maximum achievable photovoltage in organic solar cells. *Nature Communications* 2020; **11(1)**, 1488.

[58] AJ Hameed, M Ibrahim and H ElHaes. Computational notes on structural, electronic and QSAR properties of *[*C60*]* fulleropyrrolidine-1-carbodithioic acid 2; 3 and 4-substituted-benzyl esters. *Journal of Molecular Structure: THEOCHEM* 2007; **809(1-3)**, 131-136.

[59] AB Ahmed. Studying the electronic characteristics and physisorption of OTS on the pure silver surfaces *(*Ag_{10}*)*, *(*Ag_{15}*)* and *(*Ag_{18}*)*. *University of Thi-Qar Journal of Science* 2023; **10(2)**, 151-159.

[60] MJ Sani. Spin-orbit coupling effect on the electrophilicity index, chemical potential, hardness and softness of neutral gold clusters*:* A relativistic ab-initio study. *HighTech and Innovation Journal* 2021; **2(1)**, 38-50.

[61] HG Kim and HJ Choi. Thickness dependence of work function, ionization energy, and electron affinity of Mo and W dichalcogenides from DFT and GW calculations. *Physical Review B: Condensed Matter and Materials Physics* 2021; **103(8)**, 085404.

[62] KA Al-ali. Theoretical study of the structural and electronic properties of the phenol, phenoxy. *University of Thi-Qar Journal of Science* 2011; **3(1)**, 89-88.

[63] J Sadlej, JC Dobrowolski and JE Rode. VCD spectroscopy as a novel probe for chirality transfer in molecular interactions. *Chemical Society Reviews* 2010; **39(5)**, 1478-1488.